PNAS
www.pnas.org

Supplementary Information for

A unique mode of keratinocyte death requires intracellular acidification

Takeshi Matsui[a,b,1,2], Nanako Kadono-Maekubo[a], Yoshiro Suzuki[c,3], Yuki Furuichi[a,b], Keiichiro Shiraga[a,4], Hiroyuki Sasaki[a], Azusa Ishida[d,e], Sonoko Takahashi[d,e], Takaharu Okada[d,e], Kiminori Toyooka[f], Jafar Sharif[g], Takaya Abe[h], Hiroshi Kiyonari[h], Makoto Tominaga[c], Atsushi Miyawaki[i], Masayuki Amagai[a,b,1]

[a] Laboratory for Skin Homeostasis, RIKEN Center for Integrative Medical Sciences, Yokohama 230-0045, Japan
[b] Department of Dermatology, Keio University School of Medicine, Tokyo 160-8582, Japan
[c] Division of Cell Signaling, National Institute for Physiological Sciences, National Institutes of Natural Sciences, Okazaki 444-8787, Japan
[d] Laboratory for Tissue Dynamics, RIKEN Center for Integrative Medical Sciences, Yokohama 230-0045, Japan
[e] Graduate School of Medical Life Science, Yokohama City University, Yokohama 230-0045, Japan
[f] Mass Spectrometry and Microscopy Unit, RIKEN Center for Sustainable Resource Science, Yokohama 230-0045, Japan
[g] Laboratory for Developmental Biology, RIKEN Center for Integrative Medical Sciences, Yokohama 230-0045, Japan
[h] Laboratory for Animal Resources and Genetic Engineering, RIKEN Center for Biosystems Dynamics Research, Kobe 650-0047, Japan
[i] Laboratory for Cell Function Dynamics, RIKEN Center for Brain Science, Wako 351-0198, Japan.

[1]To whom correspondence may be addressed. Email: takeshi.matsui@riken.jp and amagai@keio.jp.

[2]Present address: School of Bioscience and Biotechnology, Tokyo University of Technology, Tokyo, 192-0982, Japan.

[3]Present address: Department of Physiology, Iwate Medical University, Iwate 028-3964, Japan.

[4]Present address: Division of Environmental Science and Technology, Graduate School of Agriculture, Kyoto University, Kyoto 606-8502, Japan.

This PDF file includes:

Supplementary text
Supplemental table 1
Figures S1 to S9
Legends for Movies S1 to S7
SI References

Other supplementary materials for this manuscript include the following:

Movies S1 to S7

Supplementary Information

Supplemental text

Materials and Methods

Reagents

Hoechst 33342, DRAQ7, and Rhod4-AM were purchased from Thermo Fisher Scientific Inc. (Waltham, MA, USA), BioStatus Ltd (Shepshed, UK), and AAT Bioquest (Sunnyvale, CA, USA), respectively. The culture medium used in this study was an adaptation of the MCDB153 medium (Boyce *et al.*, 1987). The MCDB153 medium (pH 5.60 and pH 7.23) containing 1 μM Ca^{2+} was prepared by adding 2-(N-morpholino) ethane sulfonic acid (MES) to the medium, and its osmolarity was adjusted (Research Institute for Functional Peptides, Yamagata, Japan). MCDB153 medium with pH values 6.14 and 6.37 was prepared by mixing the MCDB153 medium with pH 5.6 and that with pH 7.23 in the ratios 3:2 and 1:1, respectively. The pmCherry-c1 vector was purchased from Takara Bio Inc. (Shiga, Japan). pN1-R-CaMP1.07 was a generous gift from Drs. Junichi Nakai and Masamichi Ohkura (Saitama University).

Mouse lines

Animal experiments were approved by the Institutional Animal Care and Use Committee of the RIKEN Yokohama Branch [2019-008(2)], Kobe Branch (A2001-03), and the National Institutes of Natural Sciences (16A074, 17A113, and 18A041). All experiments were conducted in accordance with institutional policies. GCaMP3-expressing mice (Ai38 mice) were purchased from The Jackson Laboratories [Bar Harbor, ME, USA; B6;129S-Gt(ROSA)26Sor<tm38(CAG-GCaMP3)Hze>/J (JAX14538)] (https://www.jax.org/strain/014538). K5-Cre Tg mice (Center for Animal Resources and Development (CARD) ID: 250) were kindly provided by Prof. Junji Takeda (Osaka

University) through CARD at the Institute of Resource Development and Analysis in Kumamoto University (Kumamoto, Japan)(1). The mouse line expressing GCaMP3 was generated by crossing Ai38 with keratin 5-Cre transgenic mice (1, 2). Hos:HR-1 hairless mice were purchased from Japan SLC Inc. (Hamamatsu, Japan). All the adult mice were 3–5 months old. TRPV3-deficient mice were generated using the CRISPR/Cas9 system and used for the experiments, the findings of which are shown in Fig. 4 and Fig. S7-S8. TRPV3-deficient mice were also provided generously by Dr. Ardem Patapoutian (Scripps Research Institute, La Jolla, CA, USA). They were backcrossed with Hos:HR-1 and used for the experiments, the findings of which are shown in Fig. S9 (3). We confirmed that both TRPV3 mouse lines showed the same phenotype for $[Ca^{2+}]_i$ elevation in SG1 cells.

Plasmid construction

Venus, an improved version of a yellow fluorescent protein, is sensitive to acid pH change (Nagai *et al.*, 2002). Mutation of residue 148 from histidine to glycine increases sensitivity to pH (pKa ~7.3); the resulting "pHVenus" does not show fluorescence under pH 5.5 (4). In contrast, mCherry, an improved monomeric version of a red fluorescent protein, DsRed, has a high resistance to pH (5). For ratiometric pH imaging of SG1 cell *in vivo*, we constructed a plasmid with the pHVenus-mCherry cDNA expressed under the cytomegalovirus virus (CMV) promoter (pCMV-pHVenus-mCherry). First, pSK-pHVenus was constructed by PCR amplification and subcloning from pcDNA-pHVenus into pBluescript SK(-) using the primers [5′-ATATGTCGACGCCACCATGGTGAGCAAGGGCGAGGAGCTGTTCACC-3′ (underlined: SalI site, double-underlined: KOZAK sequence) and 5′-AATTAAGCTTCTTGTACAGCTCGTCCATGCCGAGAGTGATC-3′ (underlined: HindIII)]. pSK-mCherry was constructed by PCR amplification and subcloning from pmCherry-c into pBluescript SK(-) using the primers [5′-ATATGGATCCATGGTGAGCAAGGGCGAGGAGGATAACATG-3′ (underlined: Hind III site) and 5′-AATTGCGGCCGCTTACTTGTACAGCTCGTCCATGCCGCCGGTGGAG-3′ (underlined: NotI site)]. The mCherry cDNA was excised by BamI and NotI restriction enzymes and ligated into the BamHI-NotI site of pSH-pHVenus to yield pSK-pHVenus-mCherry. The plasmid pCMV-pHVenus-mCherry was constructed as follows: pHVenus-mCherry cDNA was excised by SalI and NotI restriction enzymes from pSK-pHVenus-mCherry and ligated into the SalI-NotI sites of pcDNA3.1, where the original SalI site was deleted to yield pCMV-pHVenus-mCherry.

Intravital multiphoton excitation microscopy

All intravital images are representative results of three independent experiments. Intravital imaging of GCaMP3 and Hoechst 33342 in the ear of adult C57BL6/N mice was performed as described previously (6), with slight modifications. Briefly, 100 μL of saline solution containing 100 μg/mL Hoechst 33342 was intraepidermally injected into the ear of GCaMP3^{epi} adult mice 17 h prior to imaging. The mice were anesthetized using isoflurane (Wako; 5% for induction, 1.5% for maintenance) supplied with oxygen. The ear was attached to micro cover glass (40×50 Thickness No. 1, C040501, Matsunami Glass IND., Osaka, Japan) with an aliquot of water and fixed on a heated stage maintained at 37 °C (Leica MATS-TypeKF, Tokai Hit, Shizuoka, Japan) to warm the cooled body of anesthetized mice. Temperature of the coverglass reached 34.5°C. The inverted TCS SP8 multiphoton excitation microscope (Leica Microsystems, Wetzlar, Germany) equipped with a Fluotar VISIR 25×/NA 0.95 water immersion objective lens was used to acquire the images. A 460/50-nm emission filter was used for Hoechst 33342 imaging, and a second harmonic generation of collagen fibers and a 525/50-nm emission filter were used for GCaMP3 imaging. For image acquisition, 155-μm × 155-μm *xy* planes were scanned at a resolution of 0.303-μm per pixel, and images of 22–34 *xy* planes with 0.996-μm *z* spacing were constructed after averaging two video frames for each (*x–y)* plane; 3D stacks were acquired every 3 min. The nuclei of interfollicular SG1 cells were identified based on the fact that they appeared in the uppermost layer of the epidermis and were elongated, as indicated by the Hoechst 33342 signals of each x-y plane image.

Intravital confocal microscopy

We previously reported that intraepidermal administration of mammalian expression vectors encoding mCherry-keratin 1 into the dorsal skin of adult hairless mice followed by electroporation resulted in sporadic expression of mCherry-keratin 1 in SG cell *in vivo* (7). Here, we further optimized this protocol and successfully omitted the electroporation step, reducing skin damage.

For intravital imaging of GCaMP3 and R-CaMP1.07, we forced the expression of the fluorescent proteins via plasmid injection. Briefly, 100 μL of saline solution containing 100 μg/mL Hoechst 33342 and 50 μL of 1 mg/mL pN1-R-CaMP1.07 prepared in water was injected intraepidermally into the dorsal skin of GCaMP3^{epi} adult hairless mice at 24 and 17 h prior to imaging, respectively. Injected regions were marked using Dr. Ph.

Martin's Black Star India Ink (Salis International, Oceanside, CA, USA). The mice were anesthetized via intraperitoneal injection of medetomidine-midazolam-butorphanol mixture (0.75:4:5). The side back skin was attached to micro cover glass (40×50 Thickness No. 1, C040501, MATSUNAMI Glass IND.) with an aliquot of water and fixed on a heated stage at 37 °C (TPi-SQH26, Tokai Hit). Images were acquired using the inverted TCS SP8 confocal microscope (Leica Microsystems) equipped with an HC PL APO CS2 40×/NA 1.30 oil immersion objective lens. A 410/480-nm emission filter was used for Hoechst 33342 detection upon excitation using a 405-nm diode laser, a 495/545-nm emission filter was used for GCaMP3 detection upon excitation using a 488-nm OPSL laser, and a 580/720-nm emission filter was used for R-CaMP1.07 detection upon excitation using a 552-nm OPSL laser. For image acquisition, 387.5-μm × 387.5-μm *xy* planes were scanned at a resolution of 0.758-μm per pixel, and images of 18–23 *xy* planes with 1.501-μm *z* spacing were constructed for each *xy* plane; 3D stacks were acquired every 5 min.

For intravital imaging of pHVenus ($Venus^{H148G}$)-mCherry, we forced the expression of the fluorescent protein via plasmid injection. The pHVenus-mCherry protein was uniformly distributed in the cytoplasm of living keratinocytes (in the stratum basale, stratum spinosum, and stratum granulosum which had neutral cytoplasmic pH; Fig S3). Briefly, 50 μL of 1 mg/mL pCMV-pHVenus-mCherry in water was intraepidermally injected into the dorsal skin of adult hairless mice (Hos:HR-1) 24 h prior to imaging. Intravital images were obtained as described above except that a 420/450-nm emission filter was used for the detection of Hoechst 33342 excited using a 405-nm diode laser, a 495/538-nm emission filter was used for the detection of pHVenus excited using a 488-nm OPSL laser, and a 580/720-nm emission filter was used for the detection of mCherry excited using a 552-nm OPSL laser. For image acquisition, 290.62-μm × 290.62-μm *xy* planes were scanned at a resolution of 0.569-μm per pixel, and images of 18–30 *xy* planes with 0.996-μm *z* spacing were constructed for each *xy* plane; 3D stacks were acquired every 5 min.

For intravital imaging of GCaMP3 and Hoechst 33342 in the dorsal skin of adult TRPV3-deficient mice, 100 μL of a saline solution containing 100 μg/mL Hoechst 33342 was intraepidermally injected into the dorsal skin of TRPV3-deficient $GCaMP3^{epi}$ adult hairless mice 17 h prior to imaging. Intravital images were obtained as described above except that a 410/480-nm emission filter was used to detect Hoechst 33342 excited using a 405-nm diode laser, and a 495/570-nm emission filter was used for the detection of GCaMP3 excited using a 488-nm OPSL laser. For image acquisition, 387.5-μm × 387.5-

μm *xy* planes were scanned at a resolution of 0.758-μm per pixel, and images of 28–36 *xy* planes with 0.999-μm *z* spacing were constructed for each *xy* plane; 3D stacks were acquired every 5 min.

Electron microscopic analysis of SG1 cells

For SEM analysis, isolated SG1/2 cells from SASP-EGFP mice were suspended in an MCDB153 medium containing 1 mM EGTA. A cell aliquot was placed onto a coverslip with a grid for 30 min at 37 ºC to allow cell adherence e (Matsunami Glass Ind.). After gently removing the unattached cells, adherent cells were fixed with 1.2% glutaraldehyde (TAAB, Aldermaston, UK) in 0.1 M phosphate buffer with 10 μg/mL Hoechst 33342 for 1 h at 25 ◦C. Then, fixed and adhered SG1/2 cells were observed using an Axio Observer Z1 microscope equipped with Colibri 7 (ZEISS, Wetzlar, Germany) and a 20× dry objective lens (Plan-NEOFLUAR NA0.50, ZEISS). Hoechst 33342, EGFP, and bright-field images of cells and the grid were obtained to identify the location of SG1 and SG2 cells. Then, cells were rinsed thrice with 4% sucrose in 0.1 M phosphate buffer and post-fixed with 1% osmium tetroxide (POLYSCIENCES, Washington, PA, USA) in 0.1 M phosphate buffer for 30 min at 25 ºC. Cells were then dehydrated for 10 min with an ascending series of ethanol solutions. Dehydrated cells were then critical-point dried with a CPD030 Critical Point Dryer (BAL-TEC: Hudson, NH) and sputter-coated with an HPC-1SW Osmium Coater (Vacuum Device, Mito, Japan). Bright-field images of the remaining cells were obtained using an Axio Observer Z1. EM images of SG1 cells (positive for both EGFP and Hoechst 33342) were obtained using a SU8220 field emission-scanning electron microscope (Hitachi High Technologies Corporation, Tokyo, Japan) with a YAG-backscattered electron detector (5 kV).

Time-lapse imaging of dying SG1 cells in vitro

All time-lapse imaging results were representative of three independent experiments. Isolated SG1 cells (10^4 – 10^5 cells) isolated from $EGFP^{SG1}$ hairless mice were suspended in 8 mL of MCDB153 medium (pH 7.23) containing 1 mM EGTA (0.21 nM Ca^{2+}) and 2 μM Rhod4-AM and passed through a cell strainer (5 mL polystyrene round-bottom tube with cell strainer cap, Corning, NY, USA). The cell suspension was then centrifuged (190 *g*) for 5 min at 25 °C. The cell pellet was suspended in 300 μL of MCDB153 medium (pH 7.23) containing 1 mM EGTA (0.21 nM Ca^{2+}) and 3 μM DRAQ7. The resulting cell suspension was transferred to a culture dish with four chambers (Hi-Q^4, ibidi GmbH,

Martinsried, Germany). Hi-Q^4 dishes were centrifuged (190 *g*) for 5 min at 25 °C and incubated at 37 °C for 30 min in a Biostation IM-Q (NIKON, Ofuna, Japan). SG1 cells were then stimulated via a triple wash with 500 µL of MCDB153 medium with various pH values (5.60, 6.14, 6.37, or 7.23) and containing different concentrations of Ca^{2+} (0.21 nM: designated as "free" in this paper and 1 mM) and 3 µM DRAQ7. The concentration of Ca^{2+} in the MCDB153 medium was adjusted to 0.21 nM and 1 mM by adding $CaCl_2$ and EGTA solutions to the medium, respectively. Time-lapse images were recorded every 5 min for 18 h or 24 h at 37 °C by using a Biostation IM-Q. The time-lapse images were exported as 24-bit TIFF files. EGFP-expressing SG1 cells were automatically selected using the Macro program "Analyze particle" after determining the threshold intensity. The area intensity of the selected region of interest (ROI) was measured, and the background was reduced. A rise in the intensity of nuclear DRAQ7 indicates an increase in cell membrane permeability, often due to cell death (8). Cell membrane permeability and DNA degradation of the isolated SG1 cells (EGFP-positive cells) waere simultaneously monitored via the measurement of DRAQ7 nuclear fluorescence signals.

As for DRAQ7, the background-subtracted fluorescence intensity of each SG1 cell as a function of time, t, was first normalized so that the minimum and the maximum values would be 0 and 1, respectively. Then the normalized intensity $I_{\mathrm{DRAQ}}(t)$ of the cells under the same medium condition was all averaged to determine the average intensity $\langle I_{\mathrm{DRAQ}}(t)\rangle$ and the standard deviation $\delta I_{\mathrm{DRAQ}}(t)$. To relatively compare $[Ca^{2+}]_i$, the medium condition that gave rise to the background-subtracted highest Rhod4-AM maximum intensity was normalized to fall between 0 and 1; and the normalized intensity $\langle I_{\mathrm{Rhod}}(t)\rangle$ of the other condition(s) to was determined based on the above values, so that its maximum value became equal to the ratio of the largest values of the original background-subtracted Rhod4-AM fluorescence intensity.

Then, for quantitative analysis of cell membrane permeability and DNA degradation, $\langle I_{\mathrm{Rhod}}(t)\rangle$ and $\langle I_{\mathrm{DRAQ}}(t)\rangle$ were decomposed into a dual-sigmoidal function described by the Hill function via the nonlinear least square method using Origin 2020 (Lightstone Corp., Tokyo, Japan). In common to Rhod4-AM $\langle I_{\mathrm{Rhod}}(t)\rangle$ and DRAQ7 $\langle I_{\mathrm{DRAQ}}(t)\rangle$ probes, both the initial rise and the subsequent decay were formulated by the first and second terms on the right-hand side of the following equations:

$$\langle I_{\mathrm{Rhod}}(t)\rangle = \frac{I_1 t^{n_1}}{{\tau_{50\%}^1}^{n_1} + t^{n_1}} - \frac{I_2 t^{n_2}}{{\tau_{50\%}^2}^{n_2} + t^{n_2}} \qquad (1\text{-}1)$$

$$\langle I_{\mathrm{DRAQ}}(t)\rangle = \frac{I_{\mathrm{CM}} t^{n_{\mathrm{CM}}}}{\tau_{50\%}^{\mathrm{CM}\ n_{\mathrm{CM}}} + t^{n_{\mathrm{CM}}}} - \frac{I_{\mathrm{DNA}} t^{n_{\mathrm{DNA}}}}{\tau_{50\%}^{\mathrm{DNA}\, n_{\mathrm{DNA}}} + t^{n_{\mathrm{DNA}}}} \quad (1\text{-}2)$$

where, an intensity I_k ($0 \leqq I_k \leqq 1$) is the increment (or decrement) from $t = 0$ and a 50 % transition time $\tau_{50\%}^{k}$ is the time required for the process to stand at half of the maximum intensity. n_k is the slope factor (k: 1 or 2 for Rhod4-AM and CM or DNA for DRAQ7). All the targeted cells were individually fitted using the Levenberg-Marquardt iterative algorithm by fixing $I_1 = I_{\mathrm{CM}} = 1.0$, until the chi-square became smaller than 10^{-6}, and the best-fitted parameters of the remaining variables were derived. Then, the average and standard deviation of $\tau_{50\%}^{\mathrm{CM}}$ (cell membrane permeabilization rate), $\tau_{50\%}^{\mathrm{DNA}}$ (DNA degradation rate) and I_{DNA} (degraded DNA) was determined after the top and bottom 5 % of the best-fitted values were removed as outliers.

RNA-seq analysis of epidermal and ETA sheets

Ear of adult C57BL6/N mice (8 weeks old, female, N=3) were separated and put on 20 µl of 10 mg/mL dispase II solution (Roche Diagnostics) dissolved in 50 mM HEPES (pH 7.5) and 150 mM NaCl or 18 µg/mL recombinant exfoliative toxin-A dissolved in phosphate-buffered saline (PBS) containing 1 mM $CaCl_2$ and incubated for 15 min at 37 ºC. The entire epidermal and ETA sheets were separated and their total RNA was prepared using an RNeasy mini kit (QIAGEN, Venlo, Netherlands). Each RNA-seq library was prepared from 1 µg of total RNA using the NEB Next Ultra Directional RNA Library Prep Kit for Illumina (New England Biolabs, Ipswich, MA, USA). Libraries were quantified using the KAPA Library Quantification Kit (Illumina GA / Universal, #KK4824). Samples were multiplexed, adjusted to 2 nM, and sequenced on an Illumina HiSeq 2000 instrument. Reads were generated via 25 bp paired-end sequencing. Transcripts Per Kilobase Million (TPM) values were calculated with Salmon (8). Gene ontology (GO) for upregulated or downregulated (> or < 3-fold) genes in ETA or epidermal sheets was determined using the g:Profiler (9).

Electrophysiology

For electrophysiological analysis, we used SG1 cells isolated from epidermal sheets because of their high viability. Isolated keratinocytes containing SG1 cells were placed onto a cover glass and incubated at 33 ºC in a 5% CO_2 incubator until use. Whole-

cell patch-clamp recordings were performed immediately after keratinocyte isolation. EGFP-positive SG1 cells were selected via fluorescence microscopy for recordings. The standard bath solution contained 140 mM NaCl, 5 mM KCl, 2 mM $CaCl_2$, 2 mM $MgCl_2$, 10 mM glucose, 5 mM HEPES, and 5 mM MES (pH 7.4 or 5.4), with or without activators (see Figure legends). The pipette solution contained 140 mM CsCl, 2 mM $MgCl_2$, 5 mM EGTA, and 10 mM HEPES (pH 7.3). An Axopatch 200B amplifier (Axon Instruments, USA) was used for recordings. Data were sampled at 10 kHz with a Digidata 1440A (Axon Instruments, San Jose, CA, USA) and analyzed using the pCLAMP10 software (Axon Instruments). The membrane potential was clamped at -60 mV. Voltage ramp pulses from -100 to +100 mV (400 ms) were applied every 5 seconds. After lifting the recording cell from the cover glass, thermal stimulations were applied via changing the bath temperature with pre-heated or cooled solutions.

We did not examine TRPM4 since it is a Ca^{2+} impermeable cation channel (10). As we do not have a TRPML1-specific activator, we did not examine it further.

Generation of TRPV3-deficient mice via CRISPR/Cas9

The CRISPR/Cas9 system was used to generate TRPV3-deficient mice. The sgRNAs targeting TRPV3 were designed using guide RNA Pick up (Broad Institute): TRPV3-CRISPR-KO-1: AGGATTTGAGCCCAACCCCA; and TRPV3-CRISPR-KO-2: CACCAATGTAGACACAACGA. To construct the guide RNA template vector, we prepared target guide RNAs containing T7 promoter sequences via PCR amplification, using oligos synthesized by KOD FX Neo (TOYOBO, Osaka, Japan):
TRPV3-CRISPR-KO-1-F: 5′-CCAAGCTTTAATACGACTCACTATAG*AGGATTTGAGCCCAACCCCA*GTTTTAGAGCTAGAAATAGCAAGT-3′ (underlined: Hind III site, double-underlined: target sequence), gRNA-F101: 5′-CCAAGCTTTAATACGACTCAC-3′, gRNA-R-XbaI: 5′-CCTCTAGAAAAGCACCGACTCGGTGCCACTTTTTCAAGTTGATAACGGACTAGCCTTATTTTAACTTGCTATTTCTAGCTCTAAAAC- 3′ (underlined: XbaI site) and gRNA-R101: 5′-CCTCTAGAAAAGCACCGACTC- 3′ (underlined: XbaI site) or TRPV3-CRISPR-KO-2-F: 5′-CCAAGCTTTAATACGACTCACTATAGCACCAATGTAGACACAACGAGTTTTAGAGCTAGAAATAGCAAGT-3′ (underlined: Hind III site, double-underlined: target sequence), gRNA-F101, gRNA-R-Xba I, and gRNA-R101. PCR products were digested with Hind III and Xba I and ligated onto the Hind III-Xba I site of pUC19 to yield pUC-T7-TRPV3-KO1-

gRNA and pUC-T7-TRPV3-KO2-gRNA. The correct insertion was confirmed with DNA sequencing using the following primers: pUC-U1908: 5′-GTGGATAACCGTATTACCGCC-3′ or M13FW: 5′- GTAAAACGACGGCCAGT - 3′. pUC-T7-TRPV3-KO1-gRNA and pUC-T7-TRPV3-KO2-gRNA were used for *in vitro* transcription using a MEGAshortscript Kit (Thermo Fisher Scientific) to yield sgRNAs (TRPV3-KO1-gRNA and TRPV3-KO2-gRNA). Cas9 RNA was transcribed using the mMESSAGE mMACHINE T7 Ultra Kit (Thermo Fisher Scientific). Cas9 RNA (40 ng/μl) and gRNAs (10 ng/μl each) were dissolved in water and injected into the cytoplasm of fertilized eggs derived from male Hos:HR-1 and female C57BL6/N mice by *in vitro* fertilization. The 346 injected eggs were cultured at 37 ºC under 5% CO_2 conditions until the 2-cell stage was reached. From the injected eggs, 122 2-cell eggs were transferred into the uterus of pseudopregnant Crl:CD1 (ICR) females. Offspring were crossed with Hos:HR-1 hairless mice and genotyped. For genotyping analysis, mouse genomic DNA was extracted from the tip of tail tissues. The following primers were used to verify gene deletions: Forward: 5′-CACAGTACTTCTAGAGCCATTTAGCCTCAG-3′, Reverse: 5′-GCACTGTCTGACCTCAGATGTACTCAA-3′. Among the generated TRPV3 deficient lines, one mouse line showed an 8512 bp deletion in the TRPV3 genomic locus, resulting in a 333 bp PCR product. TRPV3 KO mice were bred for six generations to a pure Hos:HR-1 background.

Image analysis and statistics

Intravital images were analyzed using Fiji (ImageJ). Drifting of images was corrected by the script “Correct 3D Drift”. Images containing nuclei of SB or stratum granulosum (SG1) were projected by the script “MAX intensity”. Target cells or their nuclei were marked by ROI, and their average intensities were measured using the ROI manager. Background intensity was also measured in the same manner. Changes in fluorescence intensities were calculated as the average intensity of ROI of interest minus background intensity of each image.

Time-lapse images of isolated SG1 cells expressing EGFP were analyzed using Fiji and NIS-element (NIKON). First, EGFP-positive SG1 cells rich in granules, without DRAQ7 signals in the nucleus (indicative of live cells), were marked by ROI, and changes in fluorescence intensities were measured in relation to the ROI of background and calculated as above.

Statistical analysis was performed using Prism 7 (GraphPad Software) and the Mann-Whitney test of the unpaired two-tailed Student's t-test.

Supplemental Table 1. Summary of analyzed data obtained from time-lapse imaging of isolated SG1 cells

Experiment	Medium conditions	Cell membrane permeability rate $\tau_{50\%}^{\mathrm{CM}}$ (h)	DNA degradation rate $\tau_{50\%}^{\mathrm{DNA}}$ (h)	Degraded DNA (%)
#1	1 mM $[Ca^{2+}]_e$-	0.41 ± 0.15	5.232 ± 1.76	82.9 ± 15.9
(Fig 3B)	pH_e7.23	(n = 24)	(n = 20)	(n = 24)
	Free $[Ca^{2+}]_e$-	5.04 ± 2.59	17.07 ± 0.72	33.5 ± 20.9
	pH_e7.23	(n = 18)	(n = 15)	(n = 18)
#2	1 mM $[Ca^{2+}]_e$-	0.42 ± 0.09	4.55 ± 1.14	39.8 ± 31.0
(Fig 3D)	pH_e7.23	(n = 21)	(n = 15)	(n = 21)
	1 mM $[Ca^{2+}]_e$-	0.56 ± 0.12	8.32 ± 1.17	94.1 ± 8.1
	pH_e6.37	(n = 19)	(n = 17)	(n = 19)
	1 mM $[Ca^{2+}]_e$-	0.56 ± 0.21	10.06 ± 1.75	93.1 ± 12.1
	pH_e6.14	(n = 16)	(n = 14)	(n = 16)
	1 mM $[Ca^{2+}]_e$-	0.81 ± 0.21	9.84 ± 2.41	90.0 ± 12.6
	pH_e5.60	(n = 17)	(n = 16)	(n = 18)
#3	1 mM $[Ca^{2+}]_e$-	0.64 ± 0.30	9.28 ± 1.56	88.8 ± 25.2
(Fig S5)	pH_e6.14	(n = 30)	(n = 28)	(n = 30)
	Free $[Ca^{2+}]_e$ -	2.77 ± 1.28	13.57 ± 2.13	46.7 ± 36.9
	pH_e6.14	(n = 10)	(n = 6)	(n = 10)

Cell membrane permeability rate ($\tau_{50\%}^{\mathrm{CM}}$) and DNA degradation rate ($\tau_{50\%}^{\mathrm{DNA}}$) with their standard deviations (uncertainties) determined from the dual-sigmoidal curve fitting of DRAQ7 intensity shown in Fig 2F.

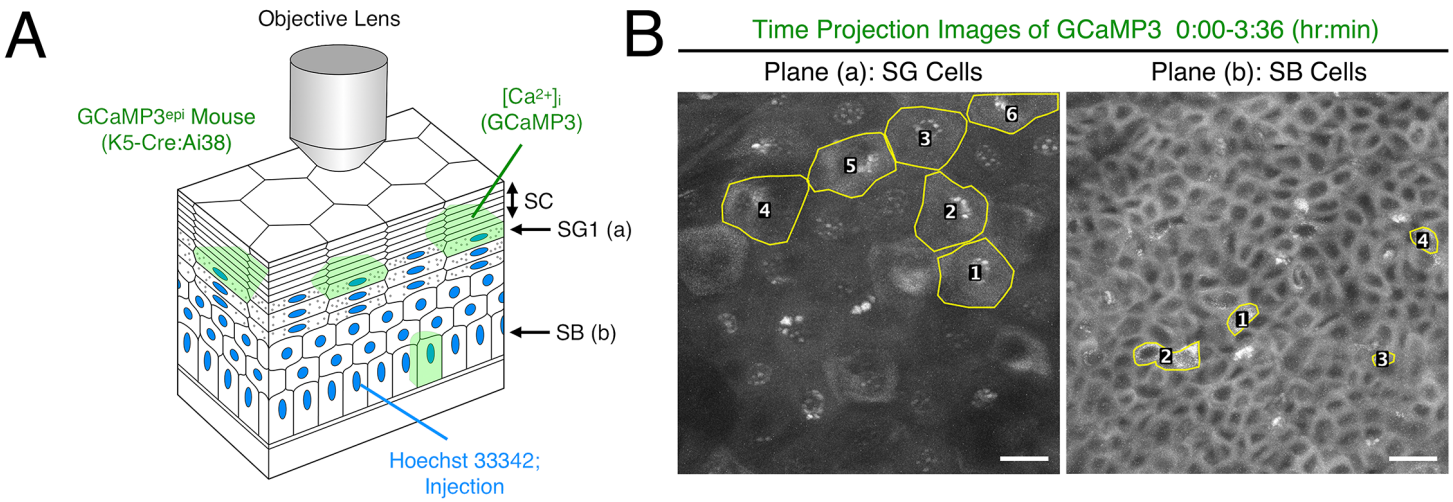

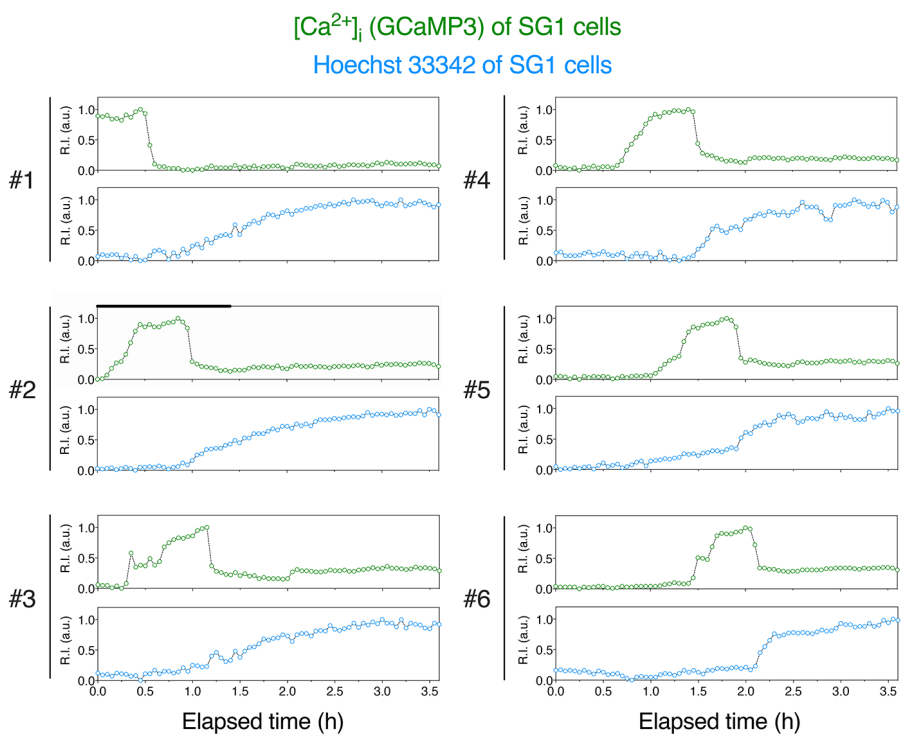

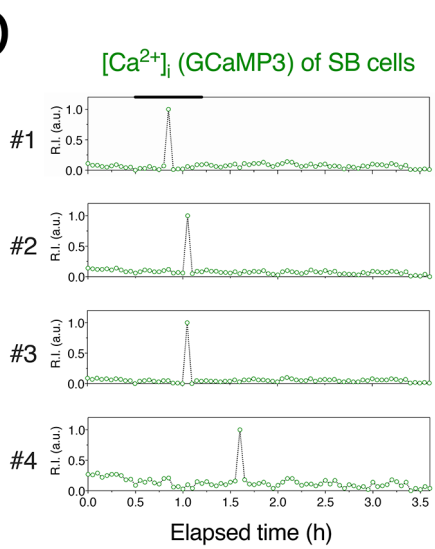

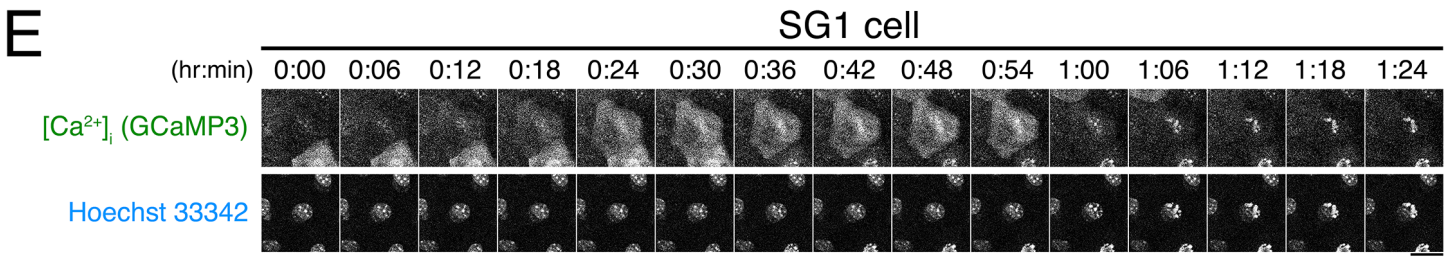

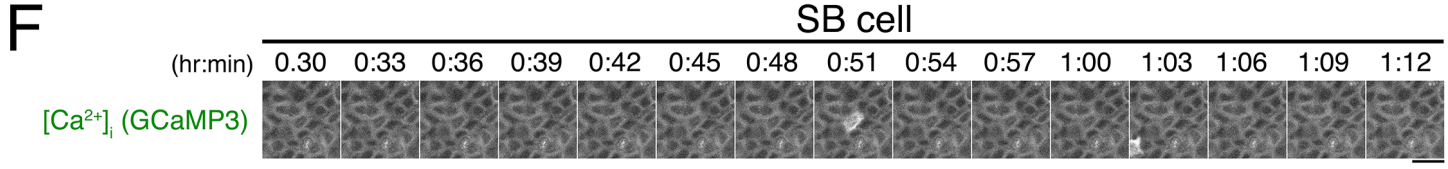

Matsui *et al.*, Figure S1

Fig. S1. Increase in $[Ca^{2+}]_i$ in SG1 cells is followed by an elevation of Hoechst 33342 signals

A. Schematic illustration of intravital GCaMP3 imaging in the ear epidermis of a $GCaMP3^{epi}$ mouse. GCaMP3 signals (green) were observed in the keratinocytes of the epidermis. Positions of SG1 and stratum basale (SB) cell layers were identified by the nuclear Hoechst 33342 signals (blue). Z-sectioning time-lapse images were obtained at 3-min intervals for 3.6 h and processed to visualize the planes of the SG1 cell layer (arrow, a) and SB cell layer (arrow, b), respectively.

B. Projection images of all of the time-lapse GCaMP3a images shown in Fig 1B-D and Movie S1 traced with the planes of SG1 (left image: Plane (a) in Fig 1B) and SB (right image: Plane (b) in Fig 1B) cells (yellow lines) in the same epidermal area that exhibited $[Ca^{2+}]_i$ elevation during intravital imaging for 3.6 h. Numbers indicate the time-dependent order of SG1 and SB cells showing increased $[Ca^{2+}]_i$. Projection images were generated from the maximum intensity, determined using ImageJ.

C. Graphs showing changes in the fluorescence intensity of GCaMP3 (green open circles) and Hoechst 33342 (blue open circles) in traced SG1 cells are shown (right graphs). Notably, after $[Ca^{2+}]_i$ was elevated in SG1 cells, the GCaMP3 signal was suddenly reduced, and the fluorescence intensity of Hoechst 33342 was inversely gradually increased. Fluorescence intensities were normalized. Title of the Y-axis; relative intensity (*R.I.*). Arbitrary unit (*a.u.*).

D. Graphs showing the time-dependent changes in the fluorescence intensity of GCaMP3 (green open circles) and Hoechst 33342 (blue open circles) in traced SB cells are shown (right graphs). Scale bar: 20 μm.

E. Representative time-lapse images of an SG cell exhibiting a single long-lasting elevation in the GCaMP3 signal and the corresponding Hoechst 33342 staining. Scale bar: 20 μm. The time-dependent change in the fluorescence intensities of GCaMP3 and Hoechst 33342 were normalized and plotted against the elapsed time. The black line indicates the duration time shown in images. See also Fig S1 and Movie S1.

F. Representative time-lapse images of an SB cell exhibiting a transient, flash-like elevation in the GCaMP3 signal. Scale bar: 20 μm. The time-dependent changes of GCaMP3 and Hoechst 33342 were plotted against the elapsed time as in (C). The black line indicates the duration time shown in images.

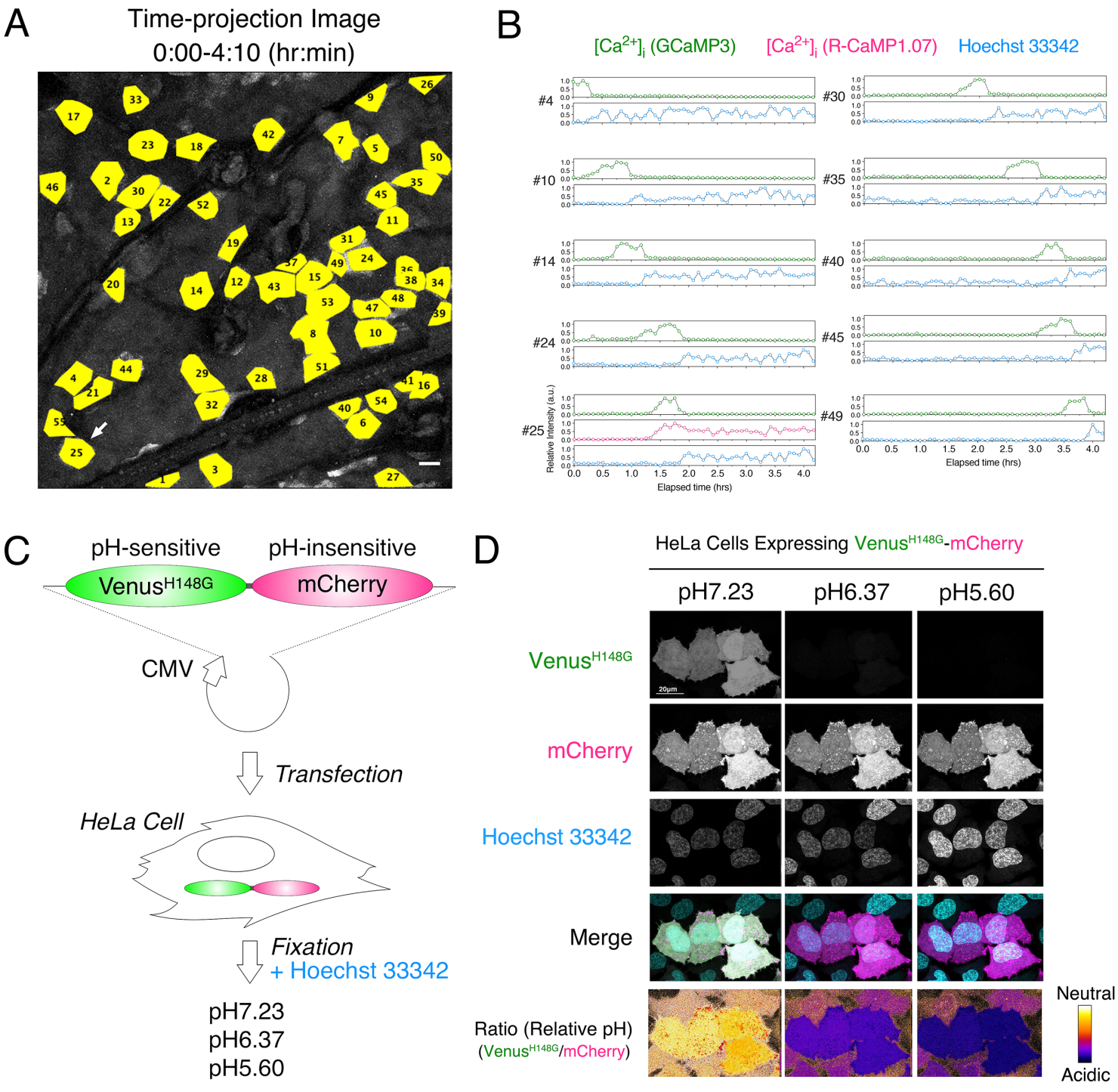

Matsui *et al.*, Figure S2

Fig. S2. Differential changes in the signals of two $[Ca^{2+}]_i$ probes, GCaMP3, and R-CaMP1.07, simultaneously expressed in SG1 cells *in vivo*

A. Projection of all time-lapse images of SG1 cells exhibiting $[Ca^{2+}]_i$ elevation for 4 h 10 min shown in Fig 2A-B and Movie S2 (filled with yellow). Numbers indicate the time-dependent order of SG1 cells showing elevation in $[Ca^{2+}]_i$. The arrow indicates an SG1 cell expressing both GCaMP3 and R-CaMP1.07 (#25 in B). Scale bar: 20 μm.

B. Graphs showing changes in the fluorescent intensity of GCaMP3 (green open circles), R-CaMP1.07 (magenta open circles), and Hoechst 33342 (blue open circles) in traced SG1 cells shown in (A) are represented. Notably, after $[Ca^{2+}]_i$ was increased in SG1 cells, the GCaMP3 signal was suddenly reduced. Conversely, the R-CaMP1.07 signal was sustained, and Hoechst 33342 fluorescence intensity gradually increased. Fluorescent intensities were normalized.

C. Schematic illustration of the analysis of the pH_{cyt} probe (pHVenus-mCherry) expressed in HeLa cells. HeLa cells were transfected with pcDNA-pHVenus-mCherry. After 24 h, the cells were fixed and stained with Hoechst 33342. Cells were then treated with pH-adjusted cultured media (pHs of 7.23, 6.37, and 5.60). Fluorescence microscopy images of pHVenus, mCherry, and Hoechst 33342 were obtained.

D. The pH-dependent changes in the fluorescence ratio of pH probes (pHVenus-mCherry) are shown. Notably, the fluorescence of pHVenus was decreased at pHs of 6.37 and 5.60, resulting in changes in the relative ratios in the image (ratio of pHVenus to mCherry signal). At a pH of 5.60, the intensity of Hoechst 33342 was increased. Scale bar; 20 μm.

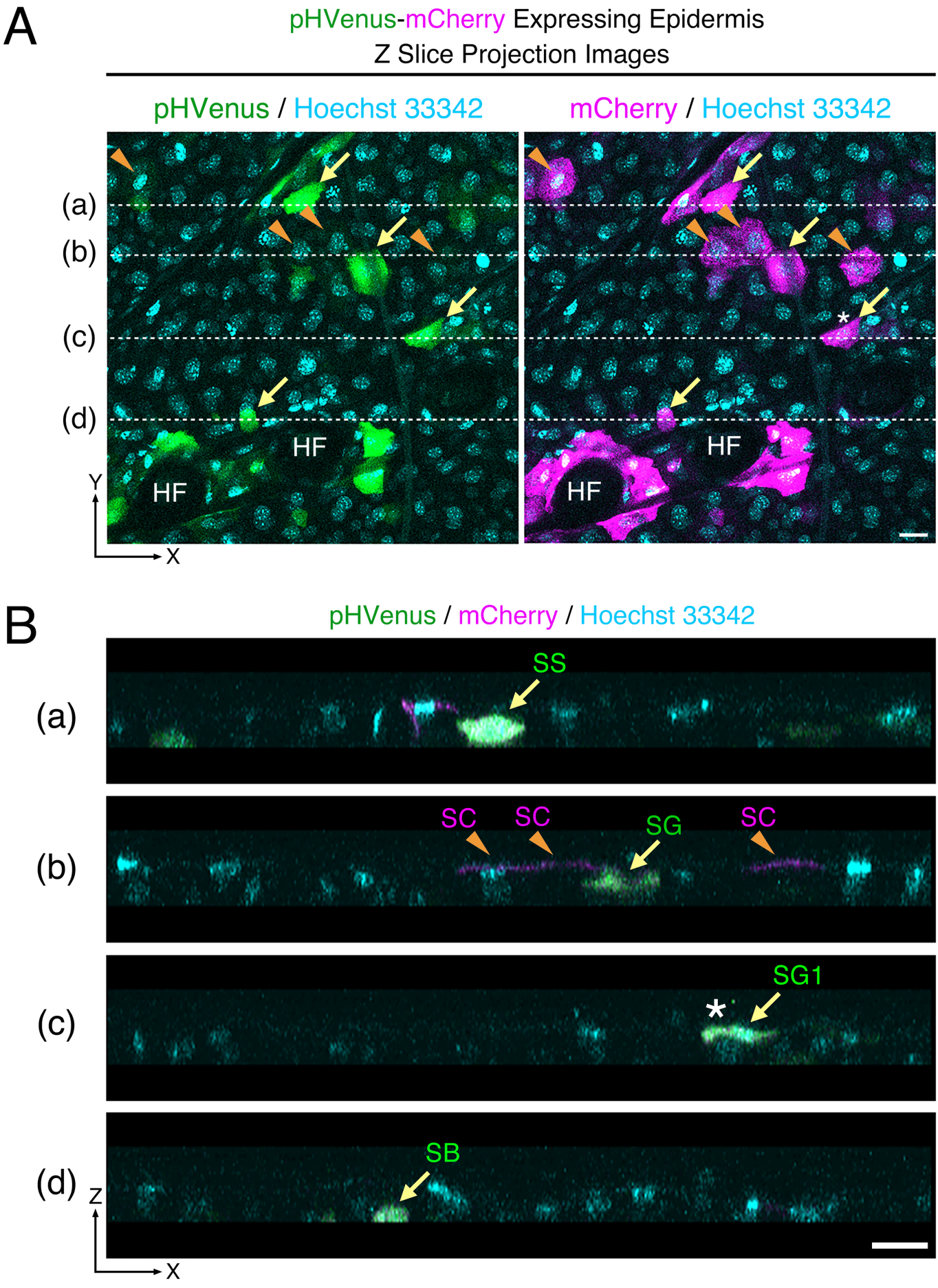

Matsui *et al.*, Figure S3

Fig. S3. Intravital visualization of pHVenus-mCherry ectopically expressed in back skin epidermis.

A. Representative *in vivo* confocal microscopic projection images of sporadically expressed pHVenus-mCherry in the dorsal skin epidermis of adult hairless mouse via intraepidermal injection of plasmid. Expressed pHVenus-mCherry signals were observed in various keratinocytes (stratum basale (SB), stratum spinosum (SS), stratum granulosum (SG) and stratum corneum (SC)). Most keratinocytes showed fluorescence of both pHVenus and mCherry (neutral pH_i; yellow arrows), whereas the corneocytes showed only mCherry signals (acidic pH_i; orange arrowheads). Dashed lines (a-d) indicates position of z-axis scanned shown in B. An asterisk indicates a SG1 cell shown in Fig 1E and Movie S3. Scale bar: 20 μm.

B. Reconstructed vertical images of z-axis scanning confocal images of A (dashed lines; a-d) Notably, SC showed only mCherry signals (acidic pH_i; orange arrowheads), whereas SB, SS and SG showed both pHVenus and mCherry signals (neutral pH_i; yellow arrows). An asterisk indicates a SG1 cell shown in Fig 1E and Movie S3. Scale bar: 20 μm.

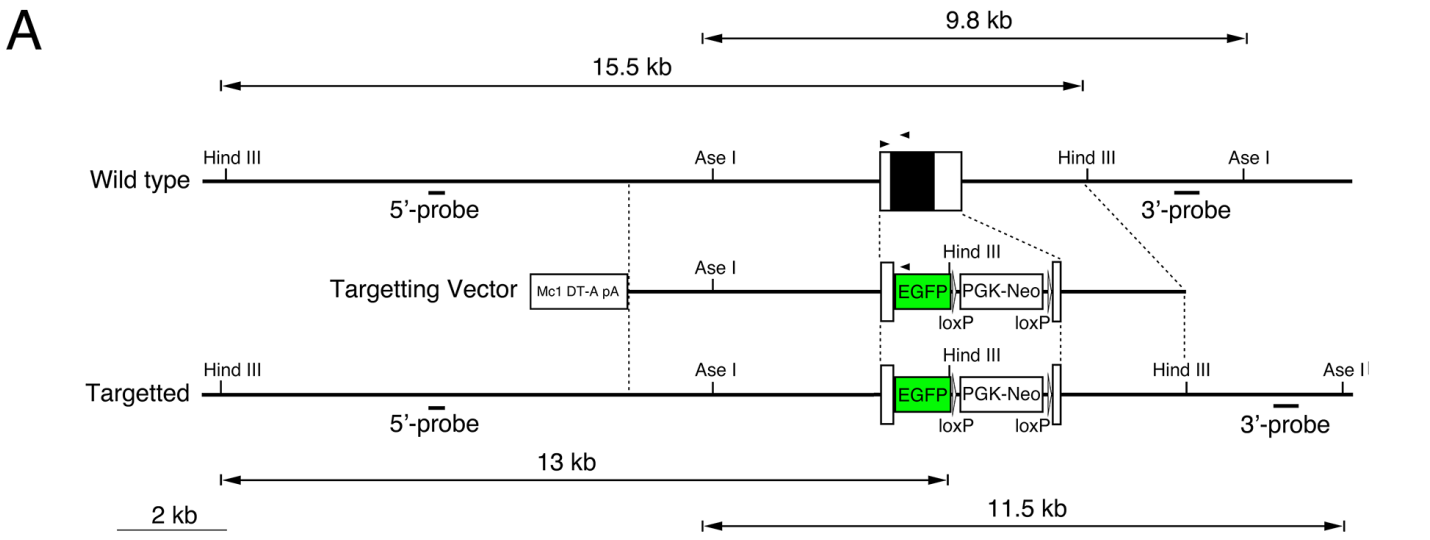

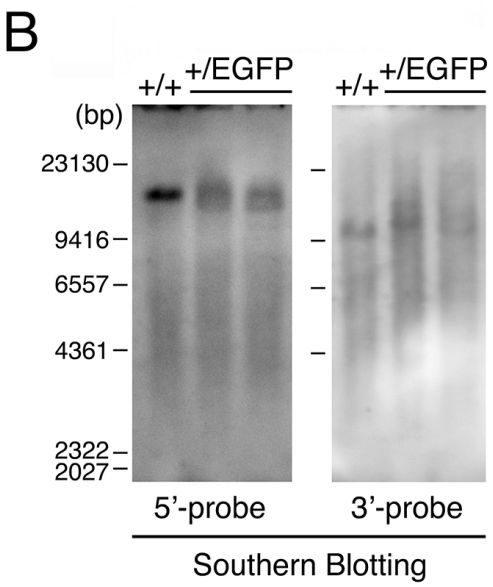

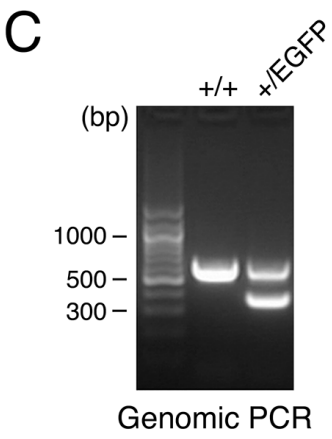

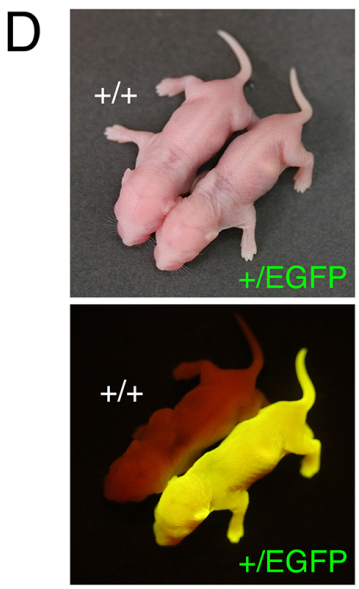

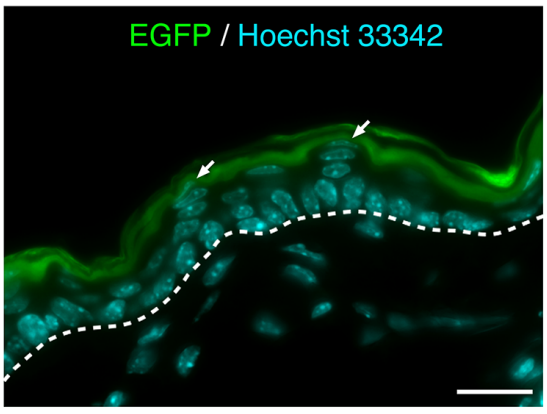

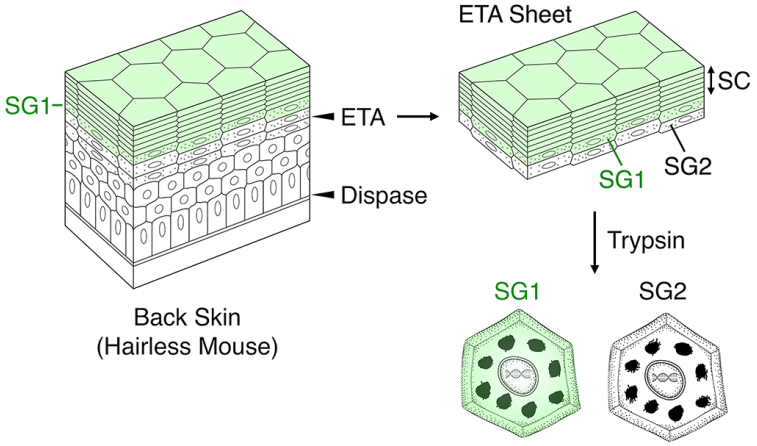

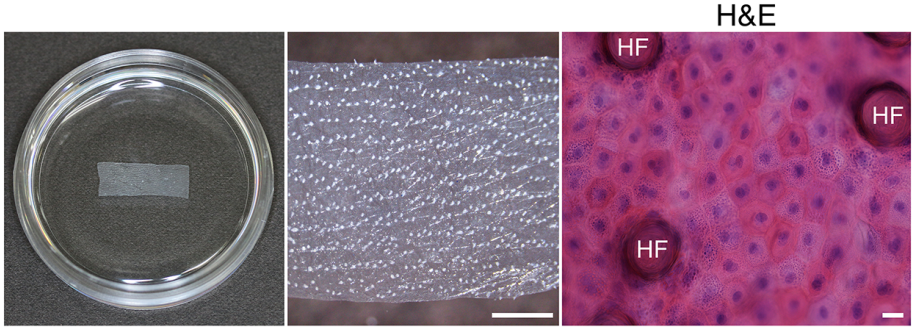

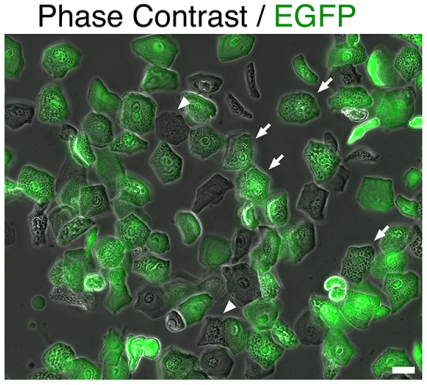

Matsui *et al.*, Figure S4

Fig. S4. Generation of the EGFP^{SG1} knock-in mouse and isolation of SG1 cells

A. Schematic representation of the EGFP^{SG1} knock-in mouse. An EGFP-Neo cassette was integrated into the SASPase/ASPRV1 gene locus on chromosome 6 in ES cells via homologous recombination. Targeted alleles exclusively expressed EGFP in the epidermal SG1 layer, under the regulation of the SASPase promoter. The black box indicates the SASPase gene open reading frame. Probes used for Southern blotting in B are indicated (5´-probe and 3´-probe). The location of primers used for genotyping is indicated via arrowheads. The PGK-Neo, cassette included the mouse phosphoglycerate kinase 1 (PGK) promoter; a neomycin resistance gene (Neo); and a mouse PGK polyA. Triangles indicate loxP sequences and their orientation. The location of fragments generated via restriction enzyme digestion is indicated by arrows.

B. Southern blots using probes described in panel A. Hind III- or Ase I-digested genomes of wild-type and heterozygous (+/EGFP) ES cells were analyzed via Southern blotting.

C. PCR amplification of genomic DNA of targeted allele (606 bp) and wild-type allele (363 bp), as shown in A.

D. Neonatal EGFP^{SG1} mice were observed under LED light. Bright fluorescence was observed on the surface skin of heterozygous (+/EGFP) mice.

E. SG1-specific expression of EGFP in the SG1 in the frozen section of the epidermal layer of heterozygous (+/EGFP) EGFP^{SG1} hairless mice. Nuclei were stained with Hoechst 33342 (cyan). The SC layer also contained the EGFP protein. Arrows indicate nuclei of SG1 cells. The dashed line indicates the border between epidermis and dermis. Scale Bar: 20 μm.

F. Procedure for isolating SG1 cells from the back skin of adult hairless mice. ETA is intraepidermally injected into the back skin. ETA sheets composed of SG1/2/SC are separated. After trypsin treatment, EGFP-positive SG1 and EGFP-negative SG2 cells rich in keratohyalin granules are cultured *in vitro*.

G. Stereomicroscopic images of an isolated ETA sheet from adult hairless mouse back skin (left and center). An isolated ETA sheet (approximately 0.5 x 1.5 cm) was floated on the 1mM $CaCl_2$/PBS in the 35 mm dish (left). HE staining of this sheet showed nuclei of polygonal SG1/2 cells rich in hematoxylin-positive granules between the inter-follicular area (right). HF: degenerated hair follicle. Scale bars; 1 mm (center), 20 μm (right).

H. Isolated SG1 (EGFP-positive; arrows; green) and SG2 (EGFP-negative; arrowheads) cells obtained from ETA sheets of adult hairless EGFP^{SG1} mice. Scale bar; 20 μm.

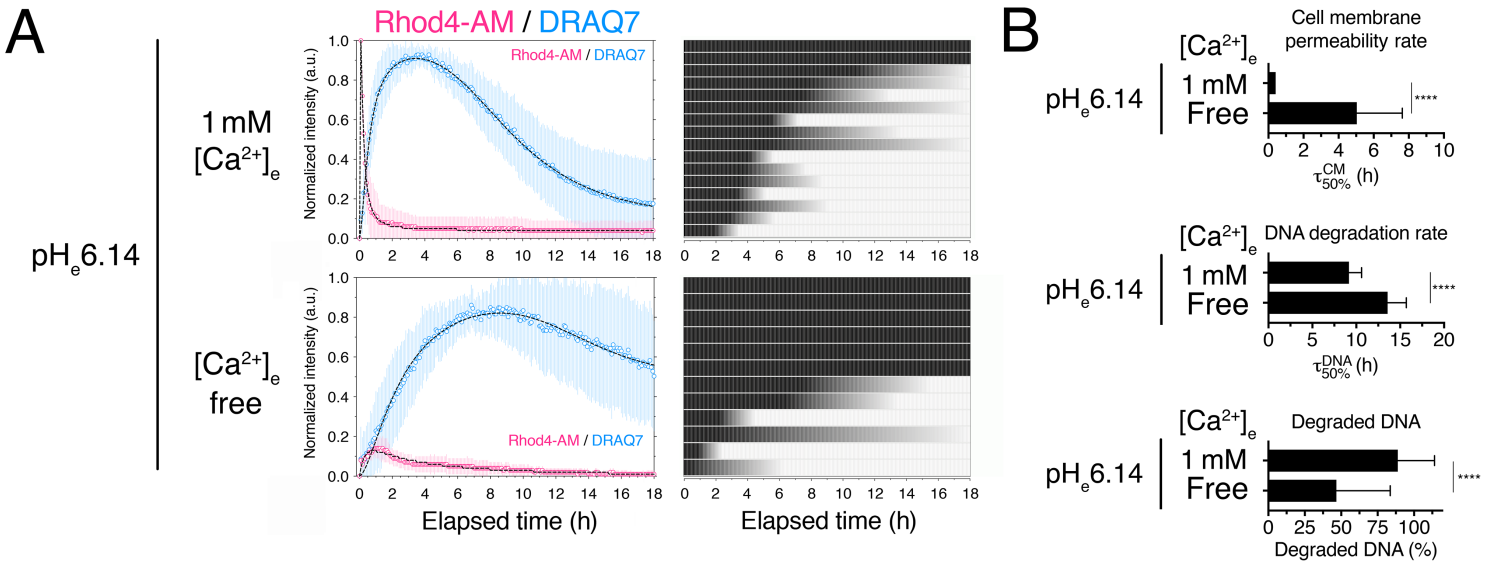

Matsui *et al.*, Figure S5

Fig. S5. Both high $[Ca^{2+}]_e$ and acidic pH_e values are required for corneocyte-related morphological changes in isolated SG1 cells *in vitro*

A. Time-dependent changes in the fluorescence intensities of Rhod4-AM and DRAQ7 in SG1 cells treated with 1 mM (n = 30) or free (n = 10) $[Ca^{2+}]_e$ under acidic pH_e conditions (pH6.14; left). The best-fit curves with the experimental intensity plot are shown by dashed lines. High $[Ca^{2+}]_e$ caused an increase in $[Ca^{2+}]_i$ followed by cell membrane permeabilization within 2 h. The gradual degradation of nuclear DNA was almost completed. In contrast, free $[Ca^{2+}]_e$ hardly induced elevations in $[Ca^{2+}]_i$ and cell membrane permeabilization. Each row of the heatmap depicts the representative time-dependent changes of the presence of KHGs (black color corresponds to an unchanged quantity of KHGs).

B. The cell membrane permeability rate ($\tau_{50\%}^{\mathrm{CM}}$) and DNA degradation rate ($\tau_{50\%}^{\mathrm{DNA}}$) derived from the dual-sigmoidal curve fitting of DRAQ7 intensity in (A). The uncertainty corresponds to the standard deviation (SD) of the derived $\tau_{50\%}$. ****$p < 0.0001$. See also Supplemental Table 1.

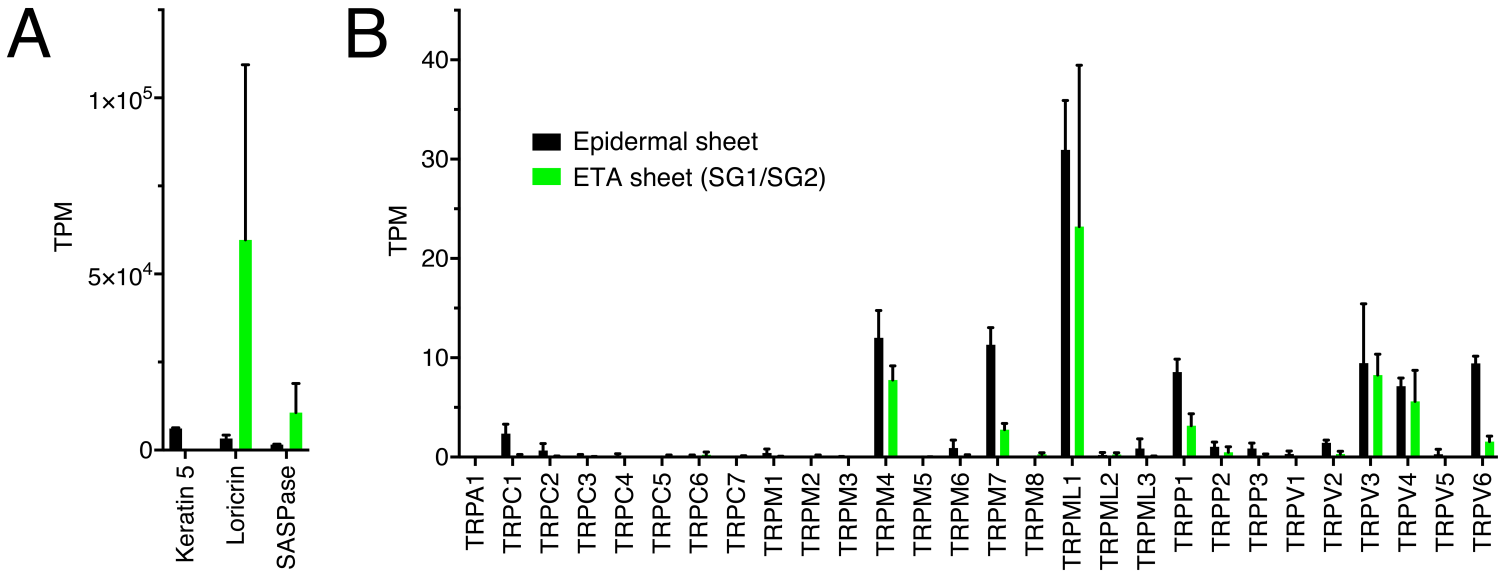

Matsui *et al.*, Figure S6

Fig. S6. Expression of genes in the epidermis and SG1/SG2 cells.

Isolated epidermal (black bars) and ETA (SG1/SG2 cells; green bars) sheets from the ear skin of adult C57BL6/N mice (8 weeks old, female) were subjected to RNA-seq analyses (n = 3 each). Loricrin and SASPase were highly expressed in SG1 and SG2 cells (A). Trpm4, Trpml1, Trpv3, and Trpv4 were also expressed in SG1 and SG2 cells (B).

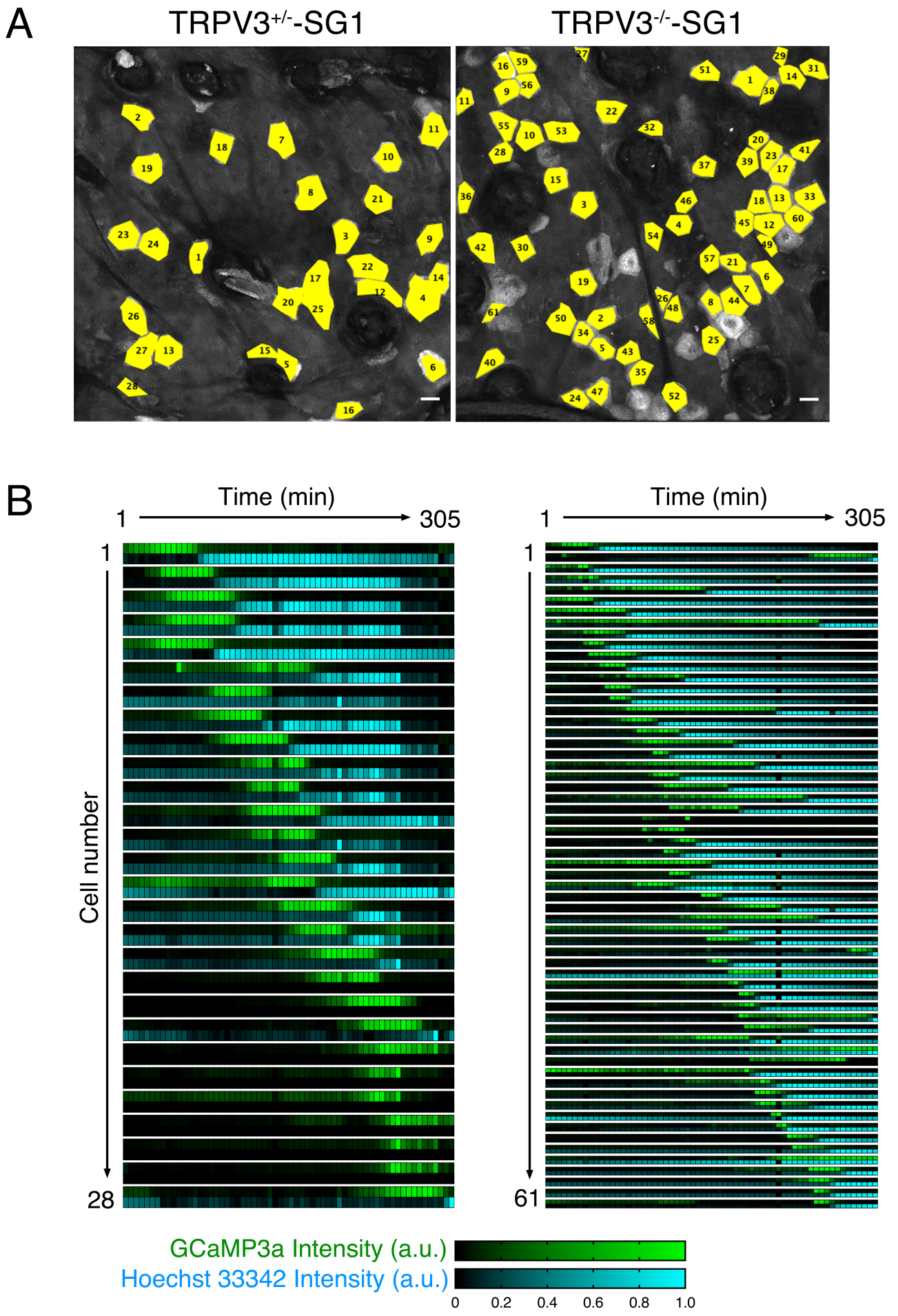

Matsui *et al.*, Figure S7

Fig. S7. $[Ca^{2+}]_i$ elevation and intracellular acidification timing were altered in TRPV3$^{-/-}$ mice

A. Projection image generated from all the time points for GCaMP3 fluorescence signals obtained from TRPV3$^{-/-}$ and TRPV3$^{-/-}$ mice expressing GCaMP3 in the epidermis (GCaMP3^{epi} mice). Numbers indicated the order of $[Ca^{2+}]_i$ elevations observed. The number of $[Ca^{2+}]_i$ elevations was increased in TRPV3$^{-/-}$ SG1 cells (n = 61) compared to TRPV3$^{+/-}$-SG1 cells (n = 28). Scale bar: 20 μm.

B. Heatmap of the time-dependent relative intensity changes in GCaMP3 (green) and Hoechst 33342 (light blue) observed in all SG1 cells in A. Fluorescence intensities were normalized. Some signals were lost due to the bleaching or loss of focus due to mice movements during intravital imaging. The frequency of $[Ca^{2+}]_i$ elevations was increased in TRPV3$^{-/-}$ mouse skin, and the timing of the decrease of GCaMP3 signals (intracellular acidification) was altered in TRPV3$^{-/-}$ mouse skin.

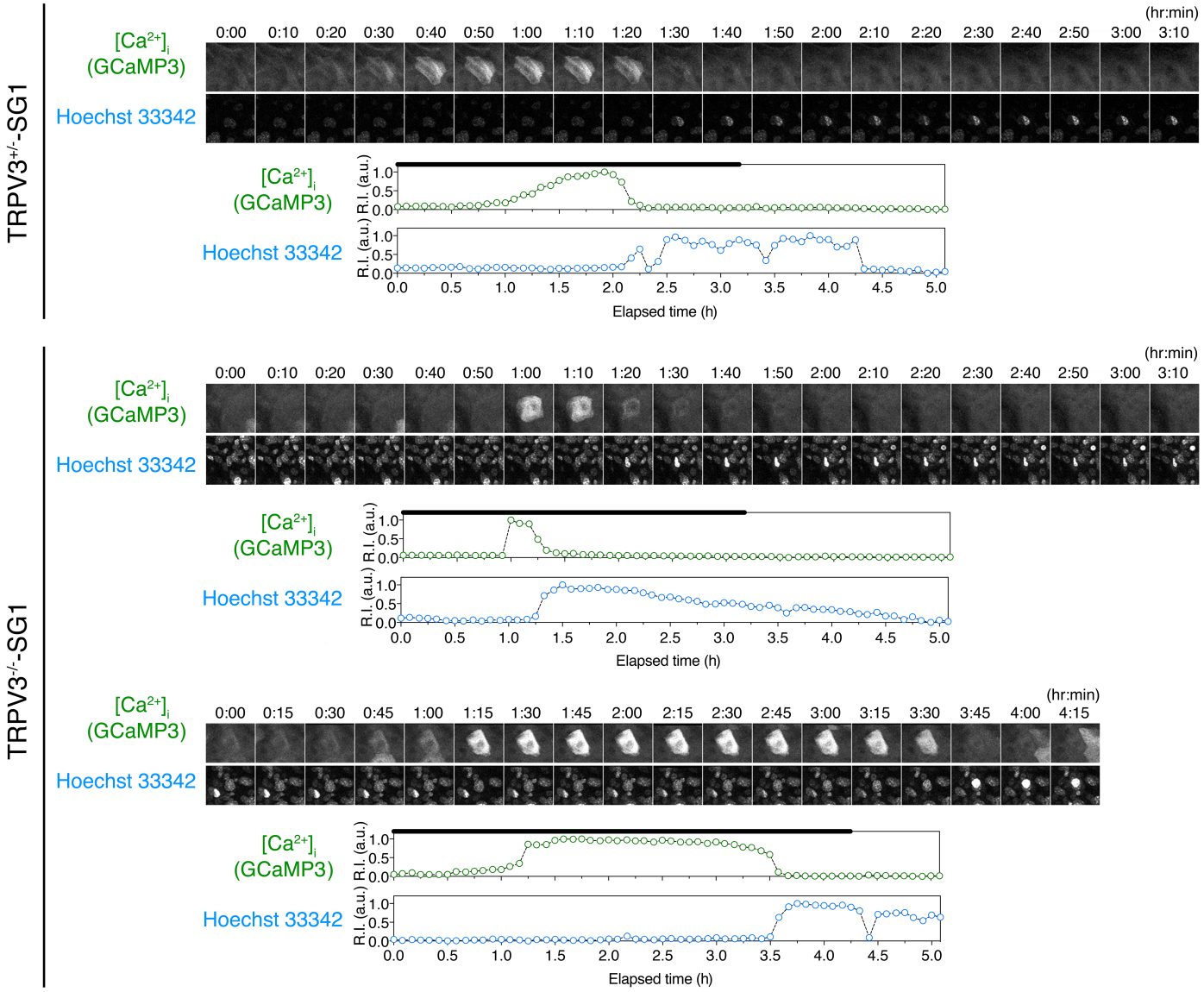

Matsui *et al.*, Figure S8

Fig. S8. Representative time-lapse images and graphs showing GCaMP3 signal intensities in TRPV3$^{+/-}$ or TRPV3$^{-/-}$ SG1 cells. The duration from the start of $[Ca^{2+}]_i$ increase, and the initiation of acidification was constant (40~60 min) in TRPV3$^{+/+}$-SG1 cells but variable in TRPV3$^{-/-}$ SG1 cells. Scale bar: 20 μm. The black line indicates the duration time shown in images.

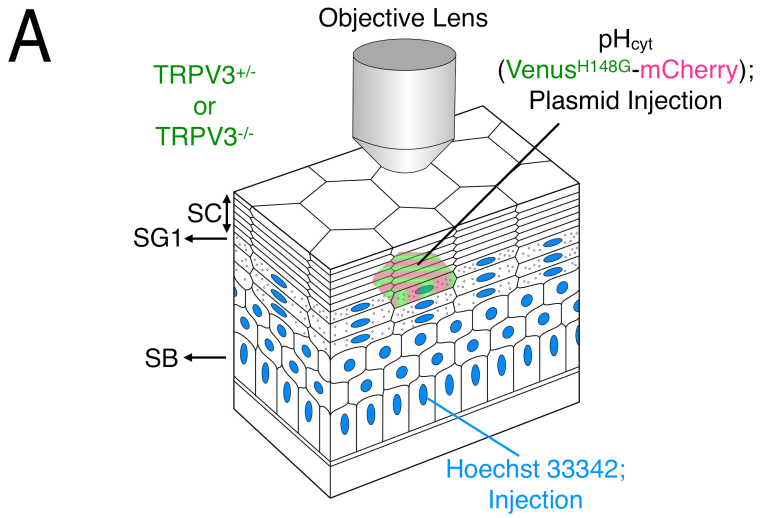
A
Objective Lens
TRPV3+/-
or
TRPV3-/-
pHcyt
(VenusH148G-mCherry);
Plasmid Injection
SC
SG1
SB
Hoechst 33342;
Injection

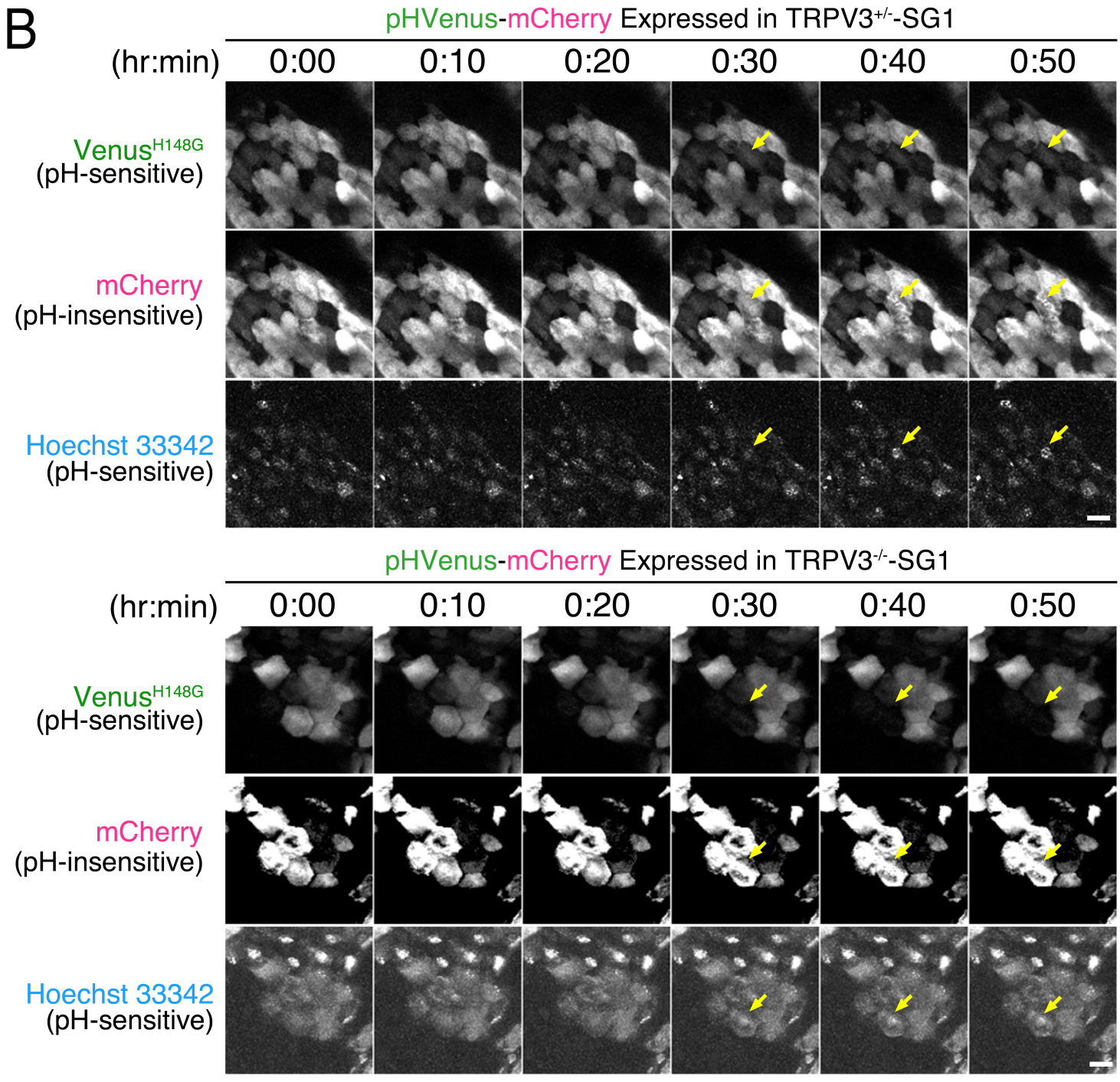
B
pHVenus-mCherry Expressed in TRPV3+/--SG1
(hr:min)
0:00
0:10
0:20
0:30
0:40
0:50
VenusH148G
(pH-sensitive)
mCherry
(pH-insensitive)
Hoechst 33342
(pH-sensitive)
pHVenus-mCherry Expressed in TRPV3-/--SG1
(hr:min)
0:00
0:10
0:20
0:30
0:40
0:50
VenusH148G
(pH-sensitive)
mCherry
(pH-insensitive)
Hoechst 33342
(pH-sensitive)

Fig. S9. Normal intracellular acidification in TRPV3$^{-/-}$-SG1 cells.

A. Schematic illustration of intravital pH_i imaging of SG1 cells expressing pHVenus-mCherry in TRPV3$^{+/-}$- or TRPV3$^{-/-}$- mice. Hoechst 33342 and the pCMV-pHVenus-mCherry plasmid were intraepidermally and sequentially injected into the dorsal skin of the adult TRPV3$^{+/-}$- or TRPV3$^{-/-}$-hairless mice.

B. Representative time-lapse images of merged view of pHVenus-mCherry ectopically expressed in SG1 cells via intraepidermal injection into dorsal skin of TRPV3-deficient hairless mice. Time-lapse images were obtained at 10-min intervals. Yellow arrows indicate SG1 cells undergo intracellular acidification. Scale Bar; 20μm.

Movie S1 Increase in $[Ca^{2+}]_i$ in SG1 cells is followed by the elevation of Hoechst 33342 intensity *in vivo*

A representative tim-lapse movie showing the changes in $[Ca^{2+}]_i$ in SG1 (plane (a) of Fig 1B) and SB (plane (b) of Fig 1B) ear skin cells of a GCaMP3^{epi} mouse. The ear skin of the GCaMP3^{epi} hairless mouse was intraepidermally injected with Hoechst 33342 17 h before intravital imaging. Time-lapse images were acquired using an inverted TCS SP8 multiphoton microscope (Leica Microsystems) at 3 min intervals for 3.6 h. GCaMP3: green, Hoechst 33342: cyan. (b) A spike-like $[Ca^{2+}]_i$ elevation was observed (arrow), whereas SG cells showed a long-lasting $[Ca^{2+}]_i$ elevation (~60 min; arrow). (b) A dividing SB cell was also observed (arrowhead). Second-harmonic generation signals corresponding to the dermal collagen also appeared in the Hoechst 33342 staining images. Scale bar: 20 μm.

Movie S2. Differential signal changes of two $[Ca^{2+}]_i$ probes, GCaMP3, and R-CaMP1.07, simultaneously expressed in SG1 cells *in vivo*

A representative time-lapse movie of the changes in $[Ca^{2+}]_i$ levels observed in mouse SG1 cells co-expressing GCaMP3 and RCaMP1.07. The dorsal skin of a GCaMP3^{epi} hairless mouse was intraepidermally injected with Hoechst 33342 and the pN-RCaMP1.07 plasmid DNA 24 h and 12 h prior to intravital imaging, respectively. Time-lapse images were acquired using an inverted TCS SP8 confocal microscope (Leica Microsystems) at 10 min intervals for 4 h 10 min. SG1 cells expressing both GCaMP3 (green) and RCaMP1.07 (magenta) showed increased fluorescence intensities (arrow). After at 1h 15 min, only the GCaMP3 signal alone was immediately decreased, whereas that of R-CaMP1.07 was sustained. Hoechst 33342 signal (cyan) was gradually increased. Time-lapse images were obtained using an SP8 at 5 min intervals for 6 h. The asterisk indicates a corneocyte expressing R-CaMP1.07 maintaining its fluorescence. Scale bar: 20 μm.

Movie S3. Gradual increase of Hoechst 33342 signal, just after the intracellular acidification of SG1 cells, *in vivo*

A representative time-lapse movie of the pH_i change observed in murine SG1 cells expressing an intracellular pH probe (pHVenus-mCherry). The back skin of a hairless mouse was intraepidermally injected with Hoechst 33342 and the pcDNA-pHVenus-mCherry plasmid DNA 24 h and 12 h prior to intravital imaging, respectively.

Horizontal image sequences (from the basal layer to the SG direction) of pHVenus-mCherry-expressing keratinocytes in the dorsal epidermis of adult hairless

mouse acquired using confocal microscopy. Green, pHVenus; Magenta, mCherry; Cyan, Hoechst 33342. Scale bar; 20 μm.

Time-lapse images were obtained using an inverted TCS SP8 confocal microscope (Leica Microsystems) at 5 min intervals for 3 h 35 min. SG1 cells from the epidermal back skin undergoing cytoplasmic acidification *in vivo*. Just after the cytoplasmic acidification, Hoechst 33342 signals begin to increase gradually. Scale bar: 20 μm.

Movie S4. Polygonal saucer-like morphology of an SG1 cell isolated from the back skin of an EGFP^{SG1} hairless mouse

A representative three-dimensional image of an isolated SG1 cell. An SG1 cell was isolated from the back skin of an EGFP^{SG1} hairless mouse, stained with Hoechst 33342 (cyan), and scanned using an inverted TCS SP8 confocal microscope (Leica Microsystems). X-Y scanning images (left movie) and reconstituted Z-section scanning images (right movie) are shown. SG1 cells show a polygonal saucer-like morphology and are rich in cytoplasmic keratohyalin granules (*KHG*). Scale bar: 10 μm.

Movie S5. High $[Ca^{2+}]_e$ and acidic pH_e values induced the elevation in $[Ca^{2+}]_i$, cell membrane permeability, KHG elimination, and DNA degradation of an isolated SG1 cell *in vitro*

A representative time-lapse movie of an isolated SG1 cell undergoing cell death. An isolated SG1 cell was treated with acidic extracellular pH (pH_e5.60) under high [Ca^{2+}] (1 mM) levels *in vitro*. Images were obtained using the BioStation IM-Q (NIKON) at 5-min intervals for 18 h 5 min. Merged snapshot image of phase-contrast and EGFP (green) before replacing the acidic medium is shown (left). Merged movie of phase-contrast, Rhod4-AM ($[Ca^{2+}]_i$; magenta), and DRAQ7 (cell membrane permeability and DNA degradation; cyan) is shown (center). Images on the extreme right are the magnified versions of the image marked using a yellow box in the middle image. Arrows indicate EGFP-positive SG1 cells. Scale bar: 10 μm.

Movie S6. Acidic pH_e values are required for the elimination of KHGs and the complete degradation of DNA in an isolated SG1 cell *in vitro*

A representative time-lapse movie of an isolated SG1 cell undergoing cell death at various extracellular pHs (pH_e7.23, 6.62, 6.37, and 5.60) under high [Ca^{2+}] (1 mM) *in vitro*. Images

were obtained via BioStation IM-Q (NIKON) at 5-min intervals for 18 h 5 min. Phase-contrast images (*Phase*), Rhod4-AM ($[Ca^{2+}]_i$), DRAQ7 (cell membrane permeability and DNA degradation), and merged images (*Merge*) are shown. Scale bar: 10 μm.

Movie S7. Aberrant frequency of $[Ca^{2+}]_i$ elevation and initiation of intracellular acidification in TRPV3$^{-/-}$ SG1 cells *in vivo*

A representative time-lapse image of SG1 cells from the back skin undergoing $[Ca^{2+}]_i$ elevation *in vivo.* Back skin of TRPV3$^{+/-}$- or TRPV3$^{-/-}$- GCaMP3^{epi} hairless mice were intraepidermally injected with Hoechst 33342 12 h prior to intravital imaging. Time-lapse images were obtained using an inverted TCS SP8 confocal microscope (Leica Microsystems) at 5 min interval for 5 h 5 min. GCaMP3: green. Hoechst 33342: cyan. Scale bars: 20 μm.

Supplementary references

1. M. Tarutani *et al.*, Tissue-specific knockout of the mouse Pig-a gene reveals important roles for GPI-anchored proteins in skin development. *Proc Natl Acad Sci U S A* **94**, 7400-7405 (1997).
2. H. A. Zariwala *et al.*, A Cre-dependent GCaMP3 reporter mouse for neuronal imaging in vivo. *J Neurosci* **32**, 3131-3141 (2012).
3. A. Moqrich *et al.*, Impaired thermosensation in mice lacking TRPV3, a heat and camphor sensor in the skin. *Science* **307**, 1468-1472 (2005).
4. T. Tojima *et al.*, Attractive axon guidance involves asymmetric membrane transport and exocytosis in the growth cone. *Nat Neurosci* **10**, 58-66 (2007).
5. N. C. Shaner *et al.*, Improved monomeric red, orange and yellow fluorescent proteins derived from Discosoma sp. red fluorescent protein. *Nat Biotechnol* **22**, 1567-1572 (2004).
6. S. Takahashi *et al.*, Homeostatic pruning and activity of epidermal nerves are dysregulated in barrier-impaired skin during chronic itch development. *Sci Rep* **9**, 8625 (2019).
7. K. Usui *et al.*, 3D in vivo imaging of the keratin filament network in the mouse stratum granulosum reveals profilaggrin-dependent regulation of keratin bundling. *J Dermatol Sci* **94**, 346-349 (2019).
8. R. Patro, G. Duggal, M. I. Love, R. A. Irizarry, C. Kingsford, Salmon provides fast and bias-aware quantification of transcript expression. *Nat Methods* **14**, 417-419 (2017).
9. U. Raudvere *et al.*, g:Profiler: a web server for functional enrichment analysis and conversions of gene lists (2019 update). *Nucleic Acids Res* **47**, W191-W198 (2019).
10. P. Launay *et al.*, TRPM4 is a Ca2+-activated nonselective cation channel mediating cell membrane depolarization. *Cell* **109**, 397-407 (2002).